



Screening and stability testing of commercially applicable *Heliotropium crispum* silver nanoparticle formulation with control over aging and biostability

Faria Khan^{1,2} · Sajid Iqbal¹ · Nauman Khalid³ · Irshad Hussain⁴ · Zajif Hussain⁴ · Rafal Szmigielski² · Hussnain A. Janjua¹

Received: 24 December 2019 / Accepted: 2 March 2020 / Published online: 29 March 2020
© King Abdulaziz City for Science and Technology 2020

Abstract

Heliotropium crispum-mediated assembly of silver nanoparticles exhibit profound antibacterial and anti-biofilm effects against multiple drug-resistant bacteria, but its stability and biocompatibility remain a hurdle in commercialization. Herein, we adopted a surface chemistry-based steric repulsion approach to investigate the colloidal stability of *H. crispum* silver nanoparticles (HC-AgNPs) and determine its application as a commercial antibacterial formulation. Two primary silver nanoparticles (AgNPs) were synthesized, i.e., HC-AgNPs and citrate-HC-AgNPs initially, which were then modulated to assemble various derivatives of AgNPs using polyethylene glycol (PEG) and polyvinylpyrrolidone (PVP) as stabilizing agents. Various parameters were assessed to investigate the morphology, colloidal physio-chemistry, and surface capping using various analytical techniques, such as UV–Vis spectrophotometer, zeta–dynamic light scattering (DLS), Fourier transform infrared spectroscopy (FTIR), scanning electron microscopy (SEM), and transmission electron microscopy (TEM). Selective AgNPs were then screened on the basis of stability for up to 8 months, heat resistance at 100 °C, and bioactivity via MTT assay using HEP-2, MCF-7, and HCEC cell lines. The UV–Vis and electron microscope results revealed that HC-AgNPs confer near-spherical and slight triangular-shaped morphology and the size of all synthesized AgNPs is in the range of 400–450 nm. All AgNPs synthesized from HC-source have characteristic FTIR peaks recorded near 2931 cm⁻¹, 1996 cm⁻¹, and 825 cm⁻¹. This study highlights promising evidence for the commercial application of HC-AgNPs as an antimicrobial agent. Additionally, it provides a methodology for modulating the surface capping of biological nanoparticles and assesses its corresponding effect on the stability.

Keywords *Heliotropium crispum* · Silver nanoparticles · Bioactivity · Surface capping · Biostability

Electronic supplementary material The online version of this article (<https://doi.org/10.1007/s13204-020-01333-x>) contains supplementary material, which is available to authorized users.

✉ Hussnain A. Janjua
hussnain.janjua@asab.nust.edu.pk

¹ Department of Industrial Biotechnology, Atta-ur-Rahman School of Applied Biosciences, National University of Science and Technology, Islamabad, Pakistan

² Institute of Physical Chemistry, Polish Academy of Sciences, Warsaw, Poland

³ School of Food and Agricultural Sciences, University of Management and Technology, Lahore, Pakistan

⁴ Department of Chemistry, SBA School of Science and Engineering (SBASSE), Lahore University of Management Sciences (LUMS), Lahore, Pakistan

Introduction

The most widely explored nanoparticles, silver, and gold, with their size-mediated optical, electronic, catalytic, and chemical properties have proved to be an impetus for a broad range of medical and biological applications (Gericke and Pinches 2006). Although the chemical approach to modulate metallic nanoparticle properties of surface chemistry and colloidal stability has been applied, the study regarding the biological method of synthesis is now being vastly explored. The synthesis of biogenic nanoparticles provides a “green” alternative to the synthesis methodology, with a less toxic and more cost-effective mode of synthesis (El-Shishtawy et al. 2011).

The exact control over size, shape, and surface capping over biologically synthesized nanoparticles is less explored

due to the least control over the synthesis process in natural extracts. Various studies suggest an effect of shape and surface capping of chemically synthesized nanoparticles on biological properties (Morgan et al. 2019). The provision of natural medium for biological nanoparticles assembly provides complex surface capping structure and colloidal stability milieu (Pinto et al. 2010). The surface chemistry of nanoparticles can be explored for broad applications by modulating its colloidal properties. In the past decades, a tremendous research effort has been carried out to evaluate the biomedical potential of noble metal-derived nanoparticles. The AgNPs are now used commercially in prosthetic devices and surgical instruments as an antibacterial agent. Its uses have been widely explored as a potential drug carrier for anti-tumor activity (Piao et al. 2011), antibacterial agent (Brown et al. 2012), and oligonucleotides synthesis (Brown et al. 2013). However, limited studies have been carried out to modify the surface chemistry of plant extract-derived AgNPs. Moreover, very little is known regarding the toxicity and biostability of AgNPs. Biofunctionalization provides subsequent control over the colloidal properties, including reactivity, solubility, and interactions in biological systems (Levard et al. 2012).

Plant extracts provide medium for strong reduction and capping of nanoparticles. Based upon the provision of physicochemical parameters, nanoparticles with various morphological properties can be assembled (Qiu et al. 2018). Although pH, temperature, and ionic agent-based size and surface capping modulation of metallic nanoparticles have been studied extensively, not much data are available on the functionalization of plant extract-mediated AgNPs synthesis (Srikanth et al. 2016). Rajput et al. reported AgNPs synthesis within the fungal system with the need to exploit organic layer to predicate the effect of surface chemistry on nanoparticles stability (Rajput et al. 2016). Various studies report that surface chemistry of AgNPs is an important factor for the determination of its fate, stability, and toxicity (Sharma et al. 2014). The colloids of AgNPs provide an indication of aggregation, dispersion, and subsequent toxicological and environmental effects (Römer et al. 2011). Chemical synthesis of AgNPs using sodium borohydride (NaBH_4) has known to induce particle aggregation with long-term storage as reported by Mulfinger et al (2007). In the current study, surface capping of previously synthesized HC-AgNPs was modulated using biocompatible polymers. AgNPs with long-term stability and high heat resistance were then screened and assessed for the evidence of any biotransformation through in vitro assay.

Materials and methods

Chemicals for AgNPs synthesis

Polyvinyl pyruvate (PVP) (Bio-basic, Canada) of average MW 40,000 and polyethylene glycol (PEG) (Appli-Chem, Germany) of average MW 4000 were used in this study. Two concentrations of 0.5 mM and 2.5 mM of PVP and PEG were prepared for further use. Details of polymers used in this study are summarized in Table S1. Sodium citrate powder ((Bio-basic, Canada) of MW 258.07 g/mol) was used in this study to prepare a 1.2 mM solution (0.3%). Furthermore, silver nitrate (AgNO_3) (Riedel de Hien, Germany) was used to prepare a 5 mM solution of AgNO_3 .

Plant extract-capped AgNPs

Plant extract-mediated synthesis was carried out using our previously described protocol (Khan et al. 2016). The concentration of plant extract was increased from 0.5 to 5.0 mg/mL, and AgNO_3 of molarity up to 5 mM was used to synthesize HC-AgNPs with enhanced capping and reduction effect.

Citrate-capped AgNPs

Citrate-AgNPs were synthesized by modifying the previously optimized chemical-based synthesis method (Romer et al. 2011). Due to the presence of plant extract-based capping agents, sodium citrate concentration used in this study was 0.3% (w/v) (1.2 mM), molarity higher than previously used study. 5 mM AgNO_3 solution was added into 1.2 mM, subsequently followed by 5.0 mg/mL plant extract (reducing agent) in 1:1:0.6 concentration, and allowed to stir on magnetic stirrer at 37 °C for 3 h.

PEG- and PVP-induced capping of citrate-AgNPs

Hoppe and his colleagues (Hoppe et al. 2006) reported the use of PVP as a reducing and capping agent to synthesize AgNPs at high temperatures. We modified the reported methodologies by adding various volumes (20–100 μL) of 0.5 mM of both PEG and PVP polymers in citrate-capped polymers (30 mL volume). The resultant mixture was homogenized through continuous stirring on the magnetic stirrer for 3 h at 40 °C.

Surface ligand exchange by PEG and PVP

Polymer-capped AgNPs were synthesized through modification of Romer et al (2011) methodology. Citrate-AgNPs were subjected to ligand exchange through the addition

of 2.5 mM PEG and PVP polymers in various volumes. 0.5 mM polymer concentration did not induce any significant capping effect, and hence, 2.5 mM PEG and PVP concentrations were used in this study to allow ligand exchange. Polymer added was increased from 5 to 25 mL in 30 mL citrate-AgNPs. The AgNPs synthesized from this adopted method was labeled as 2CPEG and 2CPVP AgNPs.

PEG- and PVP-capped AgNPs

The previously described methodology by Mulfingher et al. (2007) was modified to change the surface coating of HC-AgNPs (5.0 mg/mL of plant extract). The volume of PEG and PVP added was varied from 20 to 100 μ L of 0.5 mM concentration when reacted with 5.0 mM of AgNO_3 . The resultant mixture was kept on vigorous stirring for 3 h at 40 °C. The final details of all the reactants and their subsequent concentrations used are summarized in Table S2.

Characterization of surface-modified AgNPs

Nanoparticles were characterized through UV–Vis spectroscopy, Zeta-DLS, FTIR SEM, and TEM. The summary of the methodology and instrumentations used in this study is given in Table S3 and Section S1.

Biocompatibility and stability studies of AgNPs

The effect of high temperatures on AgNPs was studied by heating 10 mL of freshly prepared solution at 100 °C for 30 min. The effect of age on the surfactant stabilized AgNPs was studied at 4 months and 8 months of synthesis and compared to the initially synthesized AgNPs through UV–Vis spectrometer. All samples were kept in dark at room temperature.

The MCF-7 (ATCC) and HEP-2 (ATCC) cells were cultured in RPMI 1640 media, supplemented with 10% horse serum and 1% streptomycin. A fixed concentration of 1.5 mg/mL of AgNPs selected from derivative and primary AgNPs in this study was loaded into each cell culture. The viability of cells was checked at 24 h through Vybrant[®] MTT Cell Proliferation Assay Kit (V-13154) (ThermoFisher Scientific, USA). Each of the experiment was repeated four times. The fixed 1.5 mg/mL dosage concentration was decided based upon our previous studies on 0.5 HC-AgNPs on MCF-7, HEP-2, and HCEC cell lines at concentrations of 0.5–2.0 mg/mL. Statistical analysis on the data was performed using Graph Pad Prism 8.0 software. One-way ANOVA followed by Dunnett's test was performed to compare the mean of each treatment group with control group. The *p* value less than 0.5 was considered statistically significant for our studies.

Results

Characterization of primary HC-AgNPs and citrate-AgNPs

UV–Vis absorption spectrum was used to determine the optical and structural properties of AgNPs capped with *Heliotropium crispum* extract and citrate (Fig. 1a). Peak surface plasmon resonance (SPR) of 0.5 HC-AgNPs was recorded near to 437 nm. Similarly, 5.0 HC-AgNP-peaked SPR was observed at 425 nm and at 406 nm citrate-AgNPs. The single absorption curve suggests the spherical morphology of all the nanoparticles.

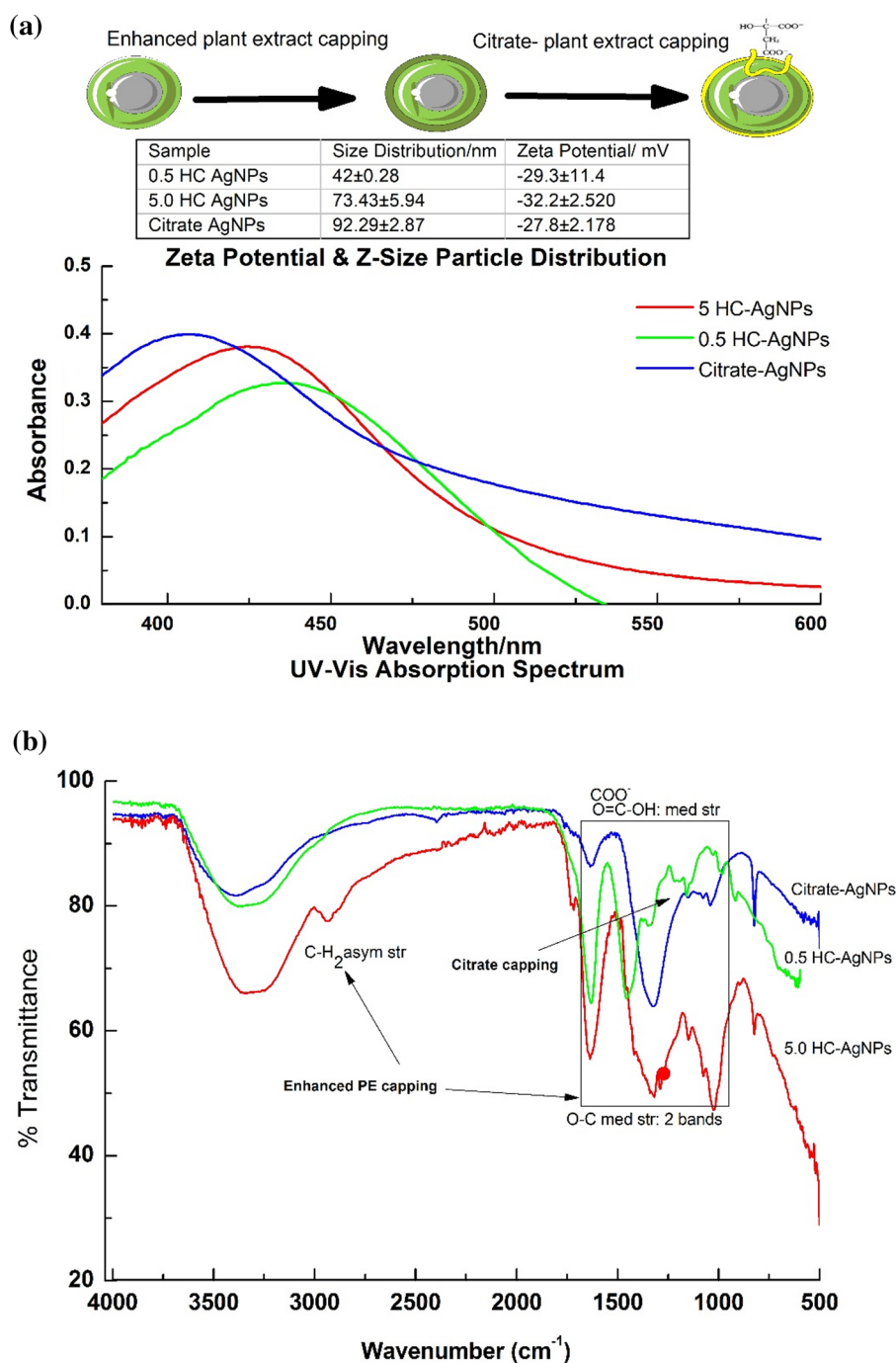
Hydrodynamic diameter (dH) of AgNPs, as observed through DLS measurement, for citrate-AgNPs was found to be 92.29 ± 2.87 nm (Polydispersity index (PDI) ≈ 0.467), while 5.0 HC-control exhibited Z-average size at 73.43 ± 5.94 nm (PDI ≈ 0.58). When compared with 0.5 HC-control (Z-average at 42 nm (PDI ≈ 0.28)), both samples exhibited an increased dH, which increased in the following manner: 0.5 HC-AgNPs > 5.0 HC-AgNPs > citrate-AgNPs.

The Ag core shape and size were determined through FE-SEM in TEM mode Fig. 1c(i–iii) which showed that in the presence of citrate, AgNPs exhibited more spherical morphology, near 400 nm. AgNPs synthesized in plant extract alone confer near-spherical and slight triangular-shaped morphology as well, thereby, contributing toward the specific peak absorbance at 425 nm. Figure 1c(i) shows near-spherical morphology of core AgNPs in 0.5 mg/mL HC sample with average particle size of 13.28 nm. The core size remained almost the same in all samples, i.e., 12.33 nm for 5 HC-AgNPs and 14.42 nm for citrate-AgNPs; hence, we can say the variation in dH size is observed due to changes in surface capping alone.

The zeta potential value suggested less the colloidal stability of 0.5 HC-AgNPs with zeta potential value ranging at -29 ± 11.4 . The Zeta values of 5.0 HC-AgNPs and citrate-AgNPs were recorded between -32 ± 2 mV and -28 ± 2 mV, respectively, in at least three independent readings, hence suggesting more colloidal stability than 0.5 HC AgNPs.

The FTIR spectrum in Fig. 1b recorded the changes in vibrational frequency due to changes in surface capping functional groups. The HC-AgNPs at 5.0 mg/mL concentration had increased plant extract-derived functional groups attached when compared with its 0.5 mg/mL counterpart. Some functional groups with a vibrational peak at 2931 cm^{-1} (C–H₂ stretch) only bind with AgNPs when present at high concentrations. Similarly, two bands at 1131 cm^{-1} and 1316 cm^{-1} corresponding to O–C-mediated bond stretches are significantly enhanced

Fig. 1 Characterization of citrate-AgNPs and HC-AgNPs at 0.5 and 5.0 mg/mL plant extract concentrations **a** UV–Vis absorption spectrum of HC-AgNPs and citrate-AgNPs. The table shows zeta potential and size distribution of 0.5HC-AgNPs, 5.0 HC-AgNPs, and citrate-AgNPs, **b** FTIR spectrum showing enhanced plant extract functional groups capping with 5.0 mg/mL concentration when compared with 0.5 mg/mL concentration. Citrate-AgNPs spectrum showing citrate functional groups (HCOO⁻, COO⁻) capping between 1500 and 1000 cm⁻¹ wavenumber and **c** FE-SEM micrographs of showing morphology through heat map with the corresponding size distribution graphs



in 5.0 HC-AgNPs. The two additional functional groups contribute toward stability of AgNPs in the aqueous plant extract.

The citrate-AgNPs nanoparticles have two types of functional groups attached: plant extract derived and citrate. The shift in infrared wavenumber at the “fingerprint region” of 1500–100 cm⁻¹ in citrate-AgNPs corresponds to citrate-derived functional groups. The binding of citrate-derived COO⁻ and COOH replaced plant extract-derived functional groups in the region.

Physiochemical characterization of derivative AgNPs

The AgNPs, surface modified through the addition of various polymer concentrations, were screened based on colloidal stability and size distribution. Figure 2 summarizes the methodology adopted for synthesis, characterization, and screening of derivative AgNPs. Details of selection criteria and characterization are shown in Supplementary section II.

Fig. 1 (continued) (c)

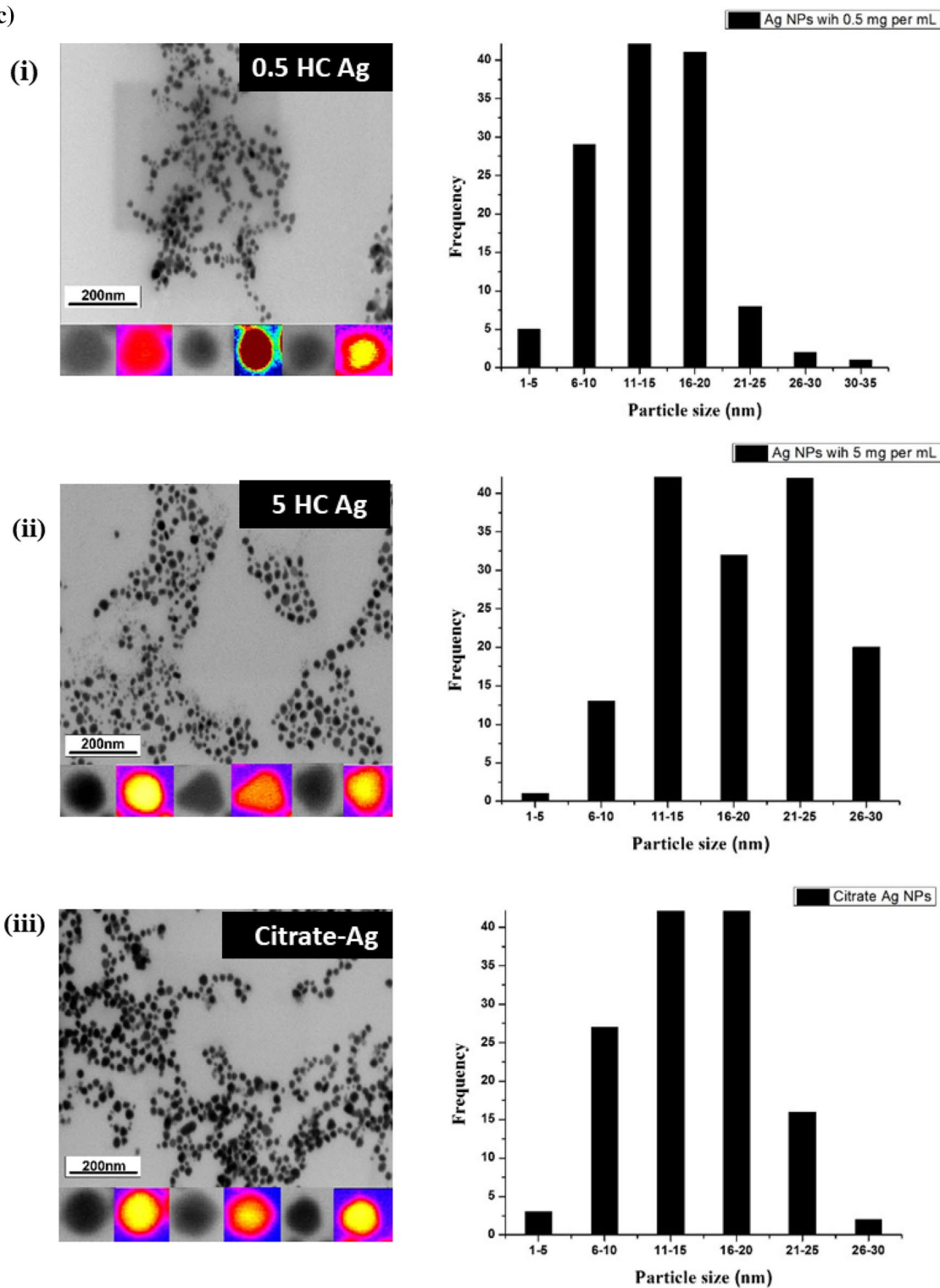
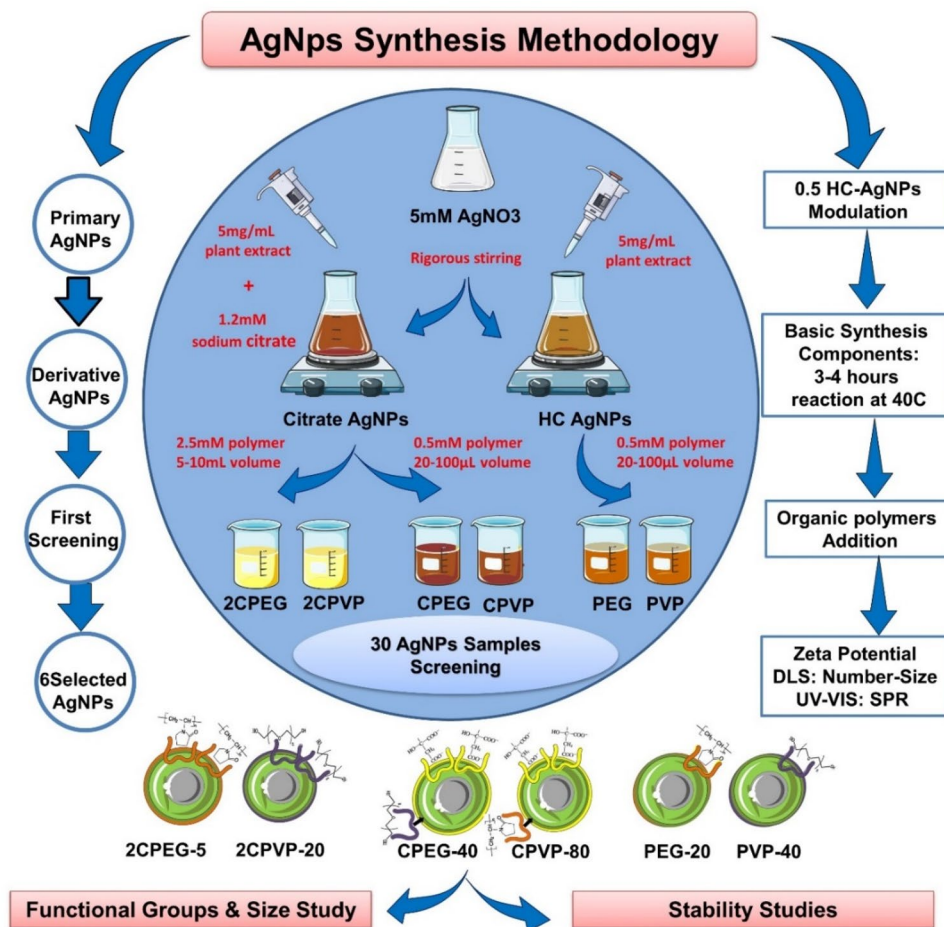


Figure 3a shows the UV–Vis absorption spectrum for CPEG-40 and CPVP-80 AgNPs, which were derived from primary citrate-AgNPs. A broader absorbance range for both CPEG-40 and CPVP-80 AgNPs indicated an increased particle size following the addition of polymers in the sample.

No significant change in core nanoparticle size was found, as confirmed through SEM images in Fig. 3a(ii) showing average particle size of CPEG-40 to be 13.47 nm and CPVP-80 near 14.84 nm, implying that increased particle size of polymer-treated AgNPs was due to change in surface coating.

Fig. 2 The synthesis methodology adopted to assemble AgNPs in HC plant extract using organic polymers and stabilizers. Note that a step by step process of synthesis was explained through which 32 various AgNPs were synthesized. During the first screening, only one AgNPs from each studied group was selected for stability studies



Similarly, the UV–Vis absorption spectrum for 2CPEG-5 and 2CPVP-20 showed absorbance peaks between 350 and 475 nm. Peak absorbance for both “derivative” AgNPs was near 412 nm, while that of citrate-AgNPs was 406 nm. The AgNPs core size of 2CPEG-5 was found to be 13.98 nm, while that of 2CPVP-20 was 16.08 nm (Fig. 3b(iii)).

When PEG and PVP polymers were added to HC-AgNPs slight redshift in absorption peak was observed for PEG-20 and PVP-40 nanoparticle colloids. The core size range of Ag in the nanoparticles, however, remains unaffected as confirmed through SEM images in Fig. 3c(ii). The average particle size for PEG-20 was found to be 15.07 nm, while that of PVP-40 was 14.10 nm, again implying the role of capping agents in the increase particle size.

As all AgNPs synthesized in this study were a modification of primary HC-AgNPs, no significant change in core Ag size was observed. Instead, the change in surface capping of “derivative” AgNPs was observed which caused a change in dH size of silver nanoparticles, and hence, the type of capping agent is the determining factor for the shift in observed size and UV–Vis absorption spectrum of AgNPs. The slight change in morphology (near-spherical of HC-AgNPs to almost all spherical of citrate-AgNPs) and unique

SPR peak attributed to citrate-AgNP-derived groups suggest that surface chemistry of AgNPs provided important details regarding specific morphology of AgNPs in the study.

Zeta potential and hydrodynamic size of stabilized derivative AgNPs

The dH of the AgNPs attributed to the core diameter and thickness of capping-agent was measured with DLS. CPEG-40. AgNPs dH was calculated to be 137 nm (PDI \approx 0.413) while CPVP-80 AgNPs dH was found to be 83.75 (PDI \approx 0.496). Zeta potential for CPEG-40 AgNPs was recorded to be -25.7 ± 2.02 mV while CPVP-80 was recorded at -13.2 ± 1.03 mV (Fig. S8b).

2CPEG-5 and 2CPVP-20 AgNPs Z-average vs intensity graph is shown in Fig. S8d. 2CPEG-5 AgNPs exhibited dH of 57.6 nm (PDI \approx 0.534), while 2CPVP-20 AgNPs had dH 104.1 nm (PDI \approx 0.45). Zeta potential for 2CPEG-5 AgNPs was recorded to be -22.0 ± 1.73 mV, while 2CPVP-20 was recorded at -20.4 ± 1.60 mV respectively (Fig. S8e). Fig. S8g shows z-distribution data for PEG-20 and PVP-80 AgNPs with corresponding HC-AgNPs control. The Z-average particle size distribution for PEG-20 was recorded at

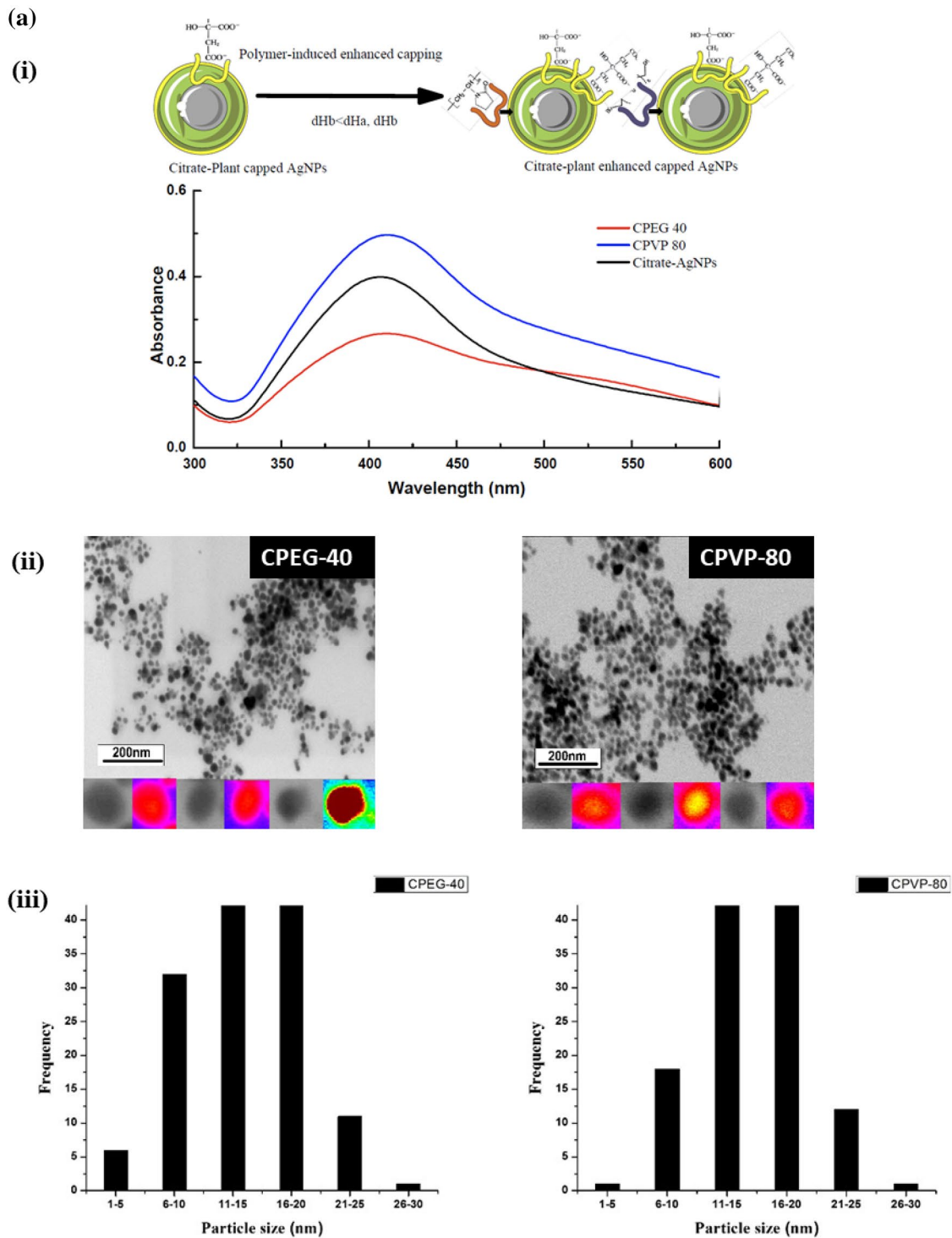
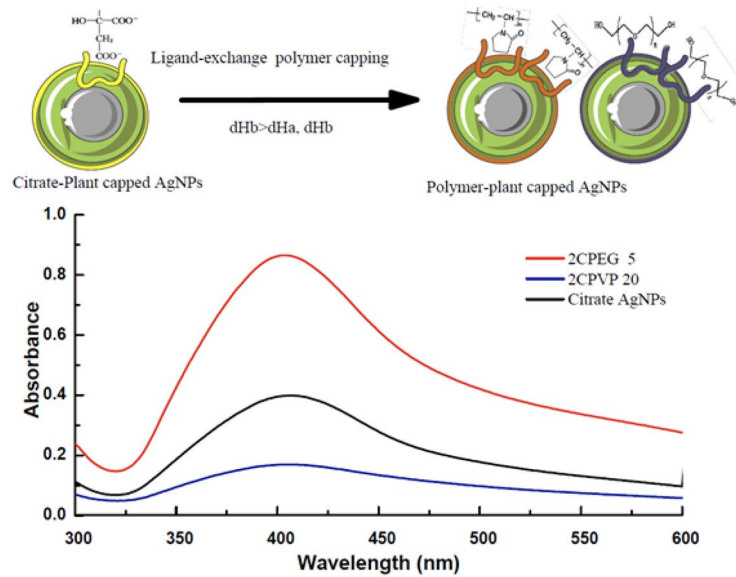


Fig. 3 UV–Vis absorption spectrum, SEM micrographs, and size distribution graphs of AgNPs treated with various stabilizing and capping agents. **a** CPEG-40 and CPVP-80 AgNPs with the corresponding citrate-AgNPs control (i) UV–Vis absorption spectrum depicting a broader absorbance peak in polymer-treated groups. This suggests increased dH for AgNPs when treated with both polymers at a lower concentration of 0.5 mM, (ii) FE-SEM image showing near-spherical nanoparticles, (iii) corresponding size distribution graphs, **b** 2CPEG-5 and 2CPVP-20 with corresponding citrate-AgNPs control

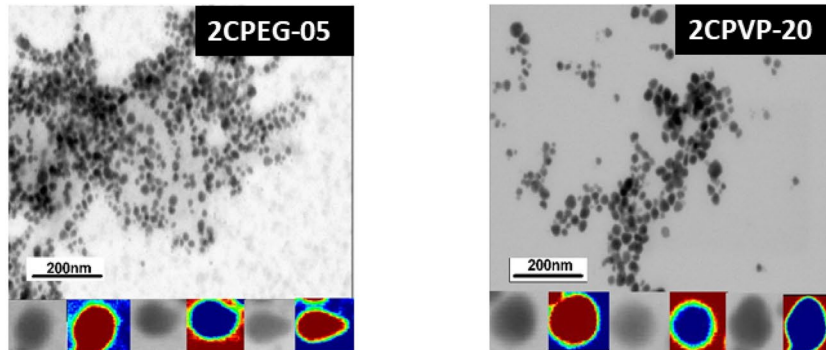
(i) absorption spectrum at almost same wavelength range of 350–475 nm exhibiting change in capping agents but not much in dH for AgNPs when treated with 5 mM of polymers, (ii) FE-SEM images, (iii) size distribution histogram, and **c** PEG-20 and PVP-40 with corresponding HC-AgNPs (i) absorption curve suggest a broader absorbance peak for polymer-treated groups. The dH for treated groups has increased considerably suggesting enhanced capping effect on AgNPs surface, (ii) SEM image showing near-spherical morphology and size range of 4–32 nm of all AgNPs, (iii) size distribution histogram

(b)

(i)



(ii)



(iii)

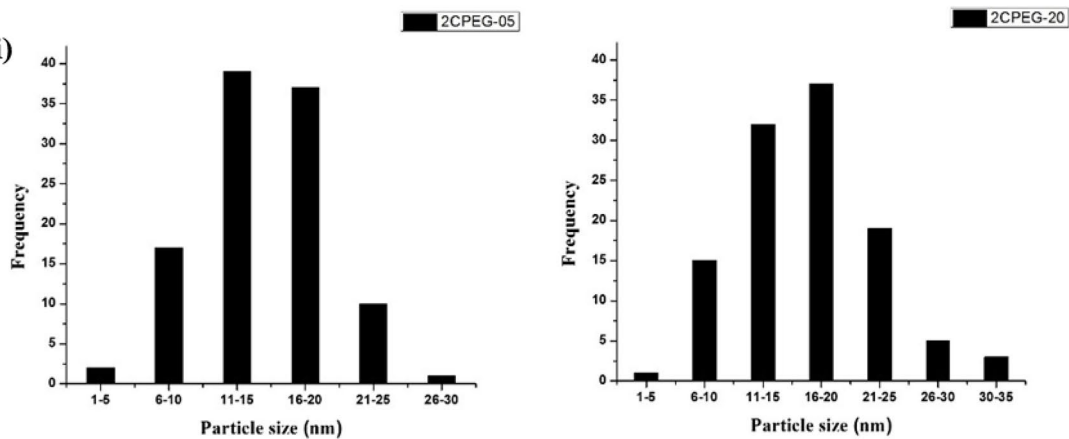


Fig. 3 (continued)

137.1 nm (PDI \approx 10.39) and at 175.6 nm (PDI \approx 0.57) for PVP-40. Zeta potential for PEG-20 AgNPs was recorded to be -16.9 ± 1.33 mV, while PVP-40 was recorded at -19.0 ± 1.49 mV (Fig. S8h).

FTIR analysis of stabilized derivative AgNPs capping agents

When the concentration of polymer was increased to

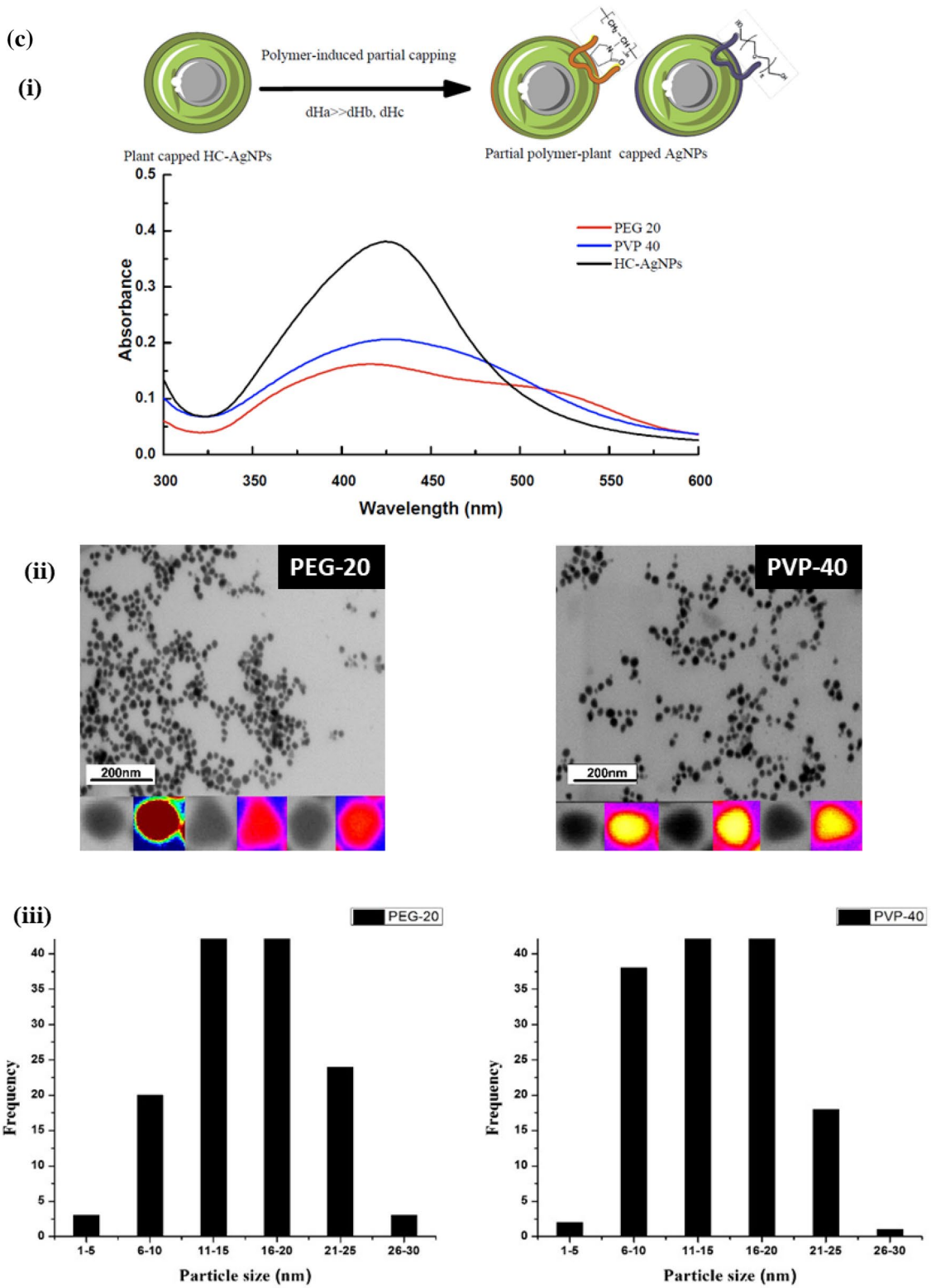


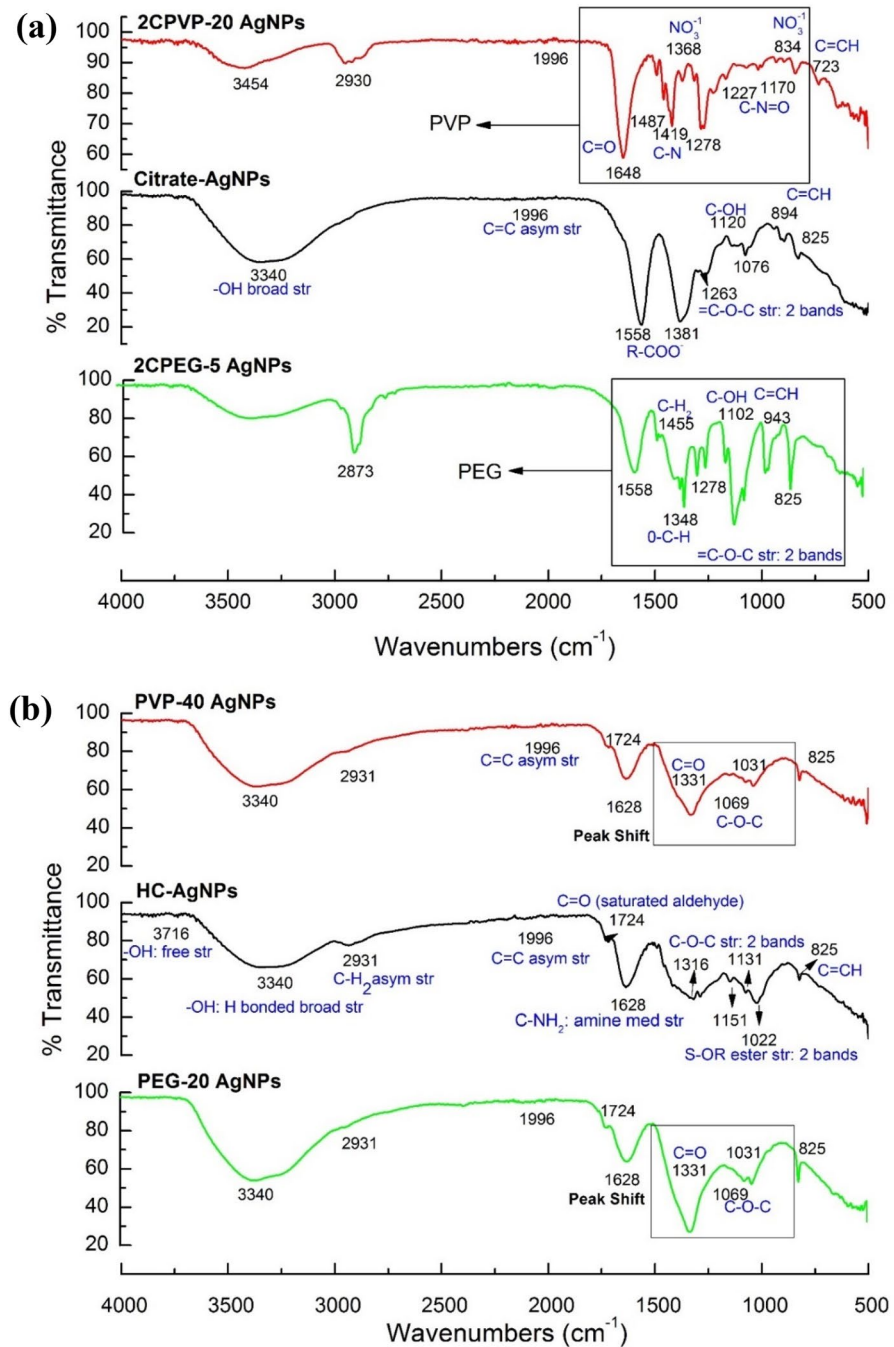
Fig. 3 (continued)

2.5 mM, ligand exchange took place and citrate from AgNPs was replaced by PEG and PVP, respectively, whereby IR peak changes took place in fingerprint regions of 1500 cm^{-1} to 1000 cm^{-1} (Fig. 4a). 2CPEG AgNPs showed IR peaks attributing toward citrate were replaced by PEG-based functional groups, whereby 1348 cm^{-1} , 1455 cm^{-1} , 1278 cm^{-1} , 1102 cm^{-1} , and 943 cm^{-1} correspond to PEG chains of O-CH, C-H₂, =C-O-C, C-OH, and C=CH, respectively. Similarly, in 2CPVP-20 AgNPs, citrate was replaced by PVP, as confirmed by the presence of functional group peaks

of PVP at 1648 cm^{-1} (C=O), $1487\text{--}1278\text{ cm}^{-1}$ (C-N), 1368 and 834 cm^{-1} (NO_3^-) and 1227 and 1170 cm^{-1} (C=N=O).

PEG and PVP polymers of 0.5 mM concentration induced a significant change in surface capping (Fig. 4b). Plant extract-derived Sulfur-ester chain was removed as well as peptide chains. Aldehyde chains at 1331 cm^{-1} was added in addition to ester C-O-C chains at 1069 cm^{-1} and 1031 cm^{-1} , respectively. This shows that less stable functional groups were detached in the presence of PVP and PEG polymers, strong reduction took place which attributed to changes in

Fig. 4 FTIR spectrum of polymer-treated AgNPs to indicate change in functional groups following polymer treatment **a** 2CPEG-5 and 2CPVP-20 AgNPs with citrate AgNPs control. A significant peak change in polymer-capped nanoparticles was observed as a function of citrate replacement from the sample followed by the appearance of IR peaks corresponding to PEG and PVP in fingerprint regions, **b** PEG-20 and PVP-40 AgNPs with HC-AgNPs control. Note that although a significant peak shift was observed in the polymer-treated nanoparticles, the new peaks do not correspond to PEG or PVP functional groups. The polymer has replaced HC-AgNPs less stable functional groups and has partially added new polymer-based functional groups (aldehyde stretch); however, plant extract-derived functional groups were so tightly bound that polymer functional groups could not replace it entirely



surface capping of AgNPs. However, the concentration of PVP-40 and PEG-20 concentration were not great enough to completely replace functional groups in HC-AgNPs at the 1500–1000 cm^{-1} fingerprint region.

The FTIR peaks of AgNPs derived from primary HC-AgNPs has characteristic IR peaks in all its subsequent polymer forms. While the changes in the fingerprint region (1500–1000 cm^{-1}) attributed toward characteristic functional groups of each type of treated AgNPs, the other FTIR spectrum remains unchanged from HC-AgNPs. The broad peak at 3340 cm^{-1} in all AgNPs contribute toward -OH derived from aqueous solvent. Similarly, peak emerges at a region between 2800 and 2900 attributing to the carbon chains (C–C, C=C) only in the presence of high polymer/plant extract concentration, suggesting increased carbon-based capping on AgNPs surface. This peak is absent in the case of 0.5 HC-AgNPs and citrate-AgNPs. Similarly, peaks emerging at 825 cm^{-1} , 895 cm^{-1} , etc. are also due to stretching vibrations of alkene groups attached to AgNPs synthesized from HC-extract.

Stability testing of AgNPs as a function of heat and aging resistance

Two parameters were studied with respect to the stability of AgNPs: aging and aggregation at high temperatures. The heat stability of AgNPs min was observed after constant boiling at 100 °C for 30. While the silver core of all AgNPs was found to be 14 ± 3 nm in the current study, the capping layer of > 50 nm was at least found in the AgNPs, conferring to high dH size. This high capping layer conferred exceptional stability to AgNPs, and hence at high temperature, only the outer capping layer susceptible to heating was removed, suggesting a decrease in silver nanoparticle size (blueshift in UV–Vis absorption spectrum). Only two groups of AgNPs—CPEG-40 and 2CPEG-5—showed red absorbance shift in absorbance spectra hence a considerable increase in particle size following heat treatment. This could be attributed to the degradation of the outer most coating layer and elongation of functional group chains specific to PEG/citrate to increase dH. The aggregation was ruled out as both groups of AgNPs presented a narrow absorbance range.

The study of stability with respect to time-revealed increased colloidal stability in all groups. Two phenomena were observed: a decrease in full width at half maximum (FWHM) and shifts in maximum absorbance (λ_{max}) with respect to time. Note that the absorbance of AgNPs increased with an increase in time was noted, implying the AgNPs nucleation and formation process preceding as time passes and degradation of AgNPs in colloid was low. The most stable of AgNPs show fewer changes in maximum absorbance with respect to time.

The AgNPs in colloid showed considerable decrease in the poly-dispersion index at 4 months as determined through FWHM graph (Fig. 5b), an indication of surface stabilization of AgNPs over a period of time. The decreased PDI in the fourth month also implies that only those class of AgNPs remained stable in the colloidal form which was highly stable, while the rest of nanoparticles degraded, and hence, narrower FWHM was observed. Citrate-AgNPs, HC-AgNPs, and PEG-20 AgNPs showed significant increase in FWHM in 8th month, suggesting a small increase in

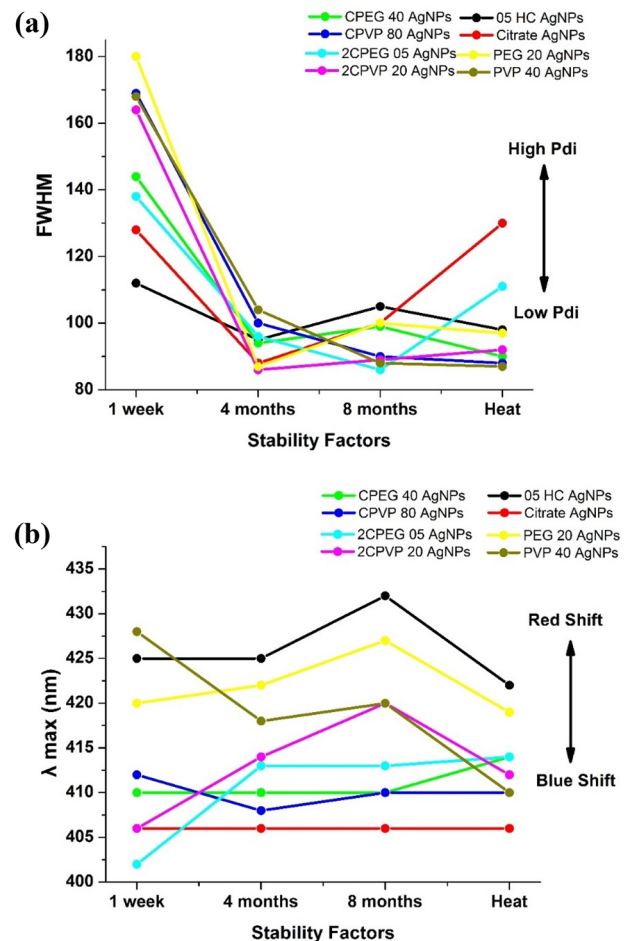


Fig. 5 Scatter-line plot exhibiting the change in maximum absorbance (λ_{max}) and full width at half maximum (FWHM) with various stability factors studied **a** λ_{max} of AgNPs. Note that most of the studied nanoparticles exhibited a blueshift in λ_{max} when heat treated at 100 °C. Also, citrate-AgNPs and its subsequent groups of AgNPs provided a blueshift in λ_{max} when compared with HC-AgNPs and its subsequent polymer groups, suggesting compact structure and bonding of citrate-AgNPs. Also, citrate-grouped AgNPs showed considerably less shift in absorbance peaks with time, while all PEG-treated AgNPs showed most variance in λ_{max} with respect to aging. **b** FWHM of AgNPs. Note that all AgNPs were generally more stabilized over time, and the lowest polydispersity index of AgNPs was observed at 4 months of synthesis, implying a gradual change in colloidal stability and size

poly-dispersion with time (Fig. 5b). Furthermore, λ_{\max} of HC-AgNPs, 2CPVP-20, and PEG-20 AgNPs also increases at 8th month suggesting redshift and increased nanoparticle size with time. Hence, after 4 months, these three AgNPs are most susceptible to aggregation and complex formation.

While λ_{\max} of citrate-AgNPs remained same throughout time, a small degree of agglomerate formation is expected at 8th month of synthesis. CPEG-40 AgNPs, CPVP-80 AgNPs, 2 CPEG-5 AgNPs, and PVP-40 AgNPs did not show a considerable change in λ_{\max} with respect to time as there was no significant change in dH observed in these sample at 4th and 8th months of synthesis.

Biocompatibility through MTT Assay

Initial assessment of dosage concentration causing a significant decrease in viability was carried out through the usage of 0.5–2.0 mg/mL dosage of 0.5 HC-AgNPs. The cellular viability was checked on three different cell lines: MCF-7, HEP-2, and HCEC.

We further used MCF-7 and HEP-2 to study the biocompatibility of primary and derivative stabilized AgNPs. Since nanoparticles could be entering through cell membrane mediated endocytosis or passive diffusion both, the comparative effect of at least two cell lines was carried out to discern if the presence of specific cellular receptors could affect cellular uptake and hence the viability of the cells.

Figure 6a represents cellular viability graphs for 0.5 HC-AgNPs implying that a slight decrease in cellular viability was observed in MCF-7 cell lines with 82% cellular proliferation even at 0.5 mg/mL dosage of AgNPs. This viability was increased to 93% upon the usage of 1.5 mg/mL of AgNPs, decreasing significantly to 79% when concentration was increased to 2.0 mg/mL.

Figure 6b represents MTT cellular viability data for AgNPs with shifts in chemical composition and diameter of capping agents than we previously studied 0.5 HC-AgNPs. Since HEP-2 and HCEC presented similar cellular viability pattern, we selected only HEP-2 cell lines for further studies. The MCF-7 response to AgNPs dosage was entirely different; hence, cellular viability was also monitored in this cell line. HEP-2 cell and HCEC cell lines exhibited an entirely different pattern of viability than that observed in MCF-7. With 0.5 mg/mL of AgNPs, more than 90% cellular viability was observed (94% and 92% respectively).

The results for cellular viability suggest that surface-capping layer composition and not the diameter of surface-capping exhibited variation in cellular response. As Ag-core size and morphology was almost the same for all the AgNPs, and the AgNPs with one of the highest diameters sizes, CPEG-40, exhibited significantly decreased proliferation response upon dosage when compared with other AgNPs. Furthermore, 2CPEG-5 AgNPs exhibited high 92%

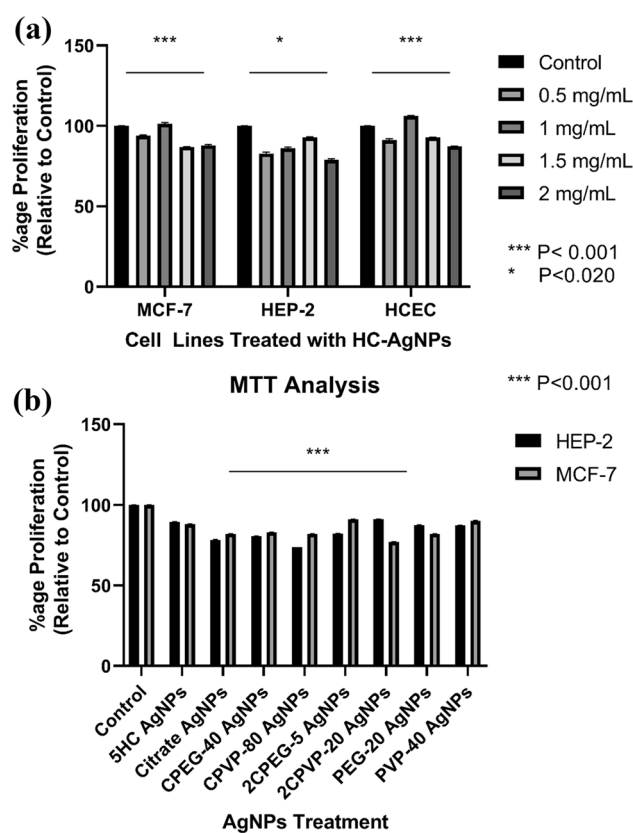


Fig. 6 Viability of cell lines assessed through MTT following dosage of various AgNPs **a** 0.5HC-AgNPs were loaded into HEP-2, MCF-7, and HCEC cell lines at the concentration ranging from 0.5–2.0 mg/mL, **b** viability assessment of polymer and stabilizer-capped primary and derivative AgNPs on HEP-2 and MCF-7 cell lines. One-way ANOVA followed by Dunnett's post hoc test was performed on each dataset to compare the mean value of each treatment with control. The p value of <0.5 was considered statistically significant

viability in MCF-7 cell lines but 82% in HEP-2. Similarly, 2CPVP-20 AgNPs viability was 77% in MCF-7, while it was 92% in HEP-2 cells. Hence, cell line-specific response was observed exhibiting more decrease in proliferation in one cell line compared to the other with the same composition and dosage of AgNPs.

PVP-40 AgNPs exhibited the highest viability in both cell lines 91% and 87%. CPEG-40 AgNPs, CPVP-80 AgNPs, and Citrate-AgNPs exhibited decreased cellular proliferation of 74–83% when compared with other AgNPs. 5HC-AgNPs and PEG-20 AgNPs exhibited a moderate decrease in viability.

Discussion

The UV–Vis absorbance peak of all the synthesized AgNPs was observed in the range of 400–450 nm which is characteristic for AgNPs (Sastry et al. 1997). The SPR is strongly

dependent on the dielectric properties of the colloid it is suspended, and many factors affect the shift in SPR peak, including synthesis substrate (HC-extract), solvent (DI water), and adsorbent (Polymers/capping functional groups) (Ravindran et al. 2013). Since the substrate and solvent concentrations were constant in this study, the SPR peak shift was attributed to the adsorbent type and concentration.

Previous studies have reported the synthesis of high yielding spherical and few triangular-shaped AgNPs in a single reactant mixture (Banerjee et al. 2014). Others have reported the presence of various morphologies (rod, triangular, and spherical) with the progression of time following synthesis (Pinto et al. 2010). The different growth rates of spheres and triangles can be attributed to different reduction kinetics of silver ions followed by attachment onto the silver particle surface (Banerjee et al. 2014).

AgNPs in a colloid are stabilized against particle aggregation through surface adsorption of polymers/functional groups or via covalent hinging of organic components. These surface modulating chains/organic groups prevent aggregation through any of the three repulsive forces between particles: electrostatic, steric, or electro-steric forces (Hotze et al. 2010).

When synthesized in biological media, at least one type of organic capping layer is found in the synthesized AgNPs. In previous studies, the use of biological extracts has been associated with the formation of AgNPs containing protein-like fragments as capping agents (de Barros et al. 2018). HC-AgNPs exhibited the presence of amine, carboxylate, and ester-mediated stretches in the finger-print regions, which are subsequently removed in the presence of other ligands/polymers. FTIR spectroscopy suggested the involvement of the amide I (C=O stretch, $1600\text{--}1700\text{ cm}^{-1}$) and amide II (CN stretch and NH deformation, $1530\text{--}1560\text{ cm}^{-1}$) in protein-coated AgNPs in previous studies as well (Ashraf et al. 2013).

All AgNPs synthesized from HC-source have characteristic FTIR peaks recorded near 2931 cm^{-1} , 1996 cm^{-1} , and 825 cm^{-1} . These peaks correspond to stretching and bending vibrations of carbon-containing chains (alkanes and alkenes), suggesting a strong capping layer presence around all AgNPs. Secondly, the broad peak at 3340 cm^{-1} regions in all AgNPs contributes toward -OH derived from an aqueous milieu of AgNPs colloid.

Previous studies reported that plant root extract-based AgNPs exhibited electro steric stabilization (Suman et al. 2013). In one study, the presence of negative charge on the surfaces of casein protein-coated AgNPs suggested that both steric and electrostatic repulsive forces in biogenic nanoparticles exist, which contribute toward its stability (Ashraf et al. 2013). The organic compounds, including citrate, however, exhibited electrostatic repulsion in the colloid. The use of organic PVP and (Huynh and Chen 2011) PEG conferred

steric repulsion in colloid when used for surface capping of nanomaterials (Kvitek et al. 2008). Hence, using a combination of organic polymers and plant extract-derived natural functional groups, both steric and electrostatic repulsions in our synthesized nano-colloids conferred the stability.

HC-AgNPs and citrate-AgNPs are surface stabilized through increased electrostatic repulsion hence we observed high negative zeta values of $-32 \pm 2\text{ mV}$ and $-28 \pm 2\text{ mV}$. The charge arises on the particle surface through the presence of negatively charged hydroxy-, oxo-, amine, or sulfide groups. As S-OR and R-O-R peaks in HC-AgNPs were replaced by citrate groups in AgNPs, a slight decrease in electrostatic negative charge could be attributed to less negative zeta value of citrate-AgNPs (El Badawy et al. 2010).

Our results indicated an increase in particle size (dH) for CPEG-40 and CPVP-80 AgNPs when compared with citrate control, indicating enhanced capping effect mediated by polymers without the removal of any functional groups from control. Similarly, 2CPEG-5 and 2CPVP-20 AgNPs exhibited a decrease in dH following polymer treatment when compared with its citrate control. This decrease in size following treatment with polymers suggests the replacement of high molecular weight functional groups from citrate-AgNPs and the addition of polymer chains to the treated groups. Likewise, polymer-treated HC-AgNPs exhibited greater dH than its plant extract-based control, which suggests the addition of polymer chains and enhanced functional group effect without the removal of any functional groups from HC-AgNPs in treated groups. The PDI ≈ 0.5 suggests that the degree of aggregation in all the samples was low.

Most steric stabilization results from the attachment of polymers in the coat, frequently as a “brush-like” layer. When this “extended” sterically hindering layer approaches another NPs surface, the translational and rotational degrees of freedom are reduced, and hence, a thermodynamically unfavorable loss in entropy is observed. The polymer layer, consequently, resists deposition and aggregation sterically. The shift in zeta potential values to more negative suggests the replacement of highly negative surface charge entities, such as those derived from citrate “hydroxy” and “oxy” groups with the polymer chains contributing toward steric repulsion (Huynh and Chen 2011). It was also noted that PEG polymers when compared with the same concentration of PVP polymer used in citrate-AgNPs ligand exchange resulted in less dH (less layer coating size) while exhibiting more negative zeta value.

Our DLS results of Z-average size distribution implies that PVP polymer causes more “brush-like” chains binding to the surface (hence increased dH) and more steric repulsion results in more shift in zeta values toward zero how these structures would contribute toward the stability of nanoparticles. Similar results were reported by Kvitek et al. in which high-molecular weight PVP proved to be

the effective AgNPs stabilizing polymer (Haberl et al. 2013; Kvittek et al. 2008). PVP molecules have little to no charge and fully coated AgNPs have been reported in the literature to exhibit a zeta potential of approximately -10 mV similar to the value reported by El Badawy (El Badawy et al. 2010). This implies that shift toward zero zeta value in case of some of PEG and PVP treated group is due to capping of PVP/PEG around AgNPs, in addition, to plant-derived functional groups.

On the other hand, studies by Zhang et al. (2012), Huynh et al. (2011), and Kelly et al. (2003) reported significantly high zeta potential values which are likely to be due to partial surface coatings of AgNPs by PVP molecules, and thus, these particles might be partially charged and partially sterically stabilized, with those studied by Huynh et al. being more charge stabilized (Afshinnia et al. 2017). The partial capping of HC-AgNPs by PEG and PVP hence having zeta value near -15 to -20 mV could be explained by electro-steric repulsion of surface capping in the colloid.

The derivative groups of AgNPs containing PEG and PVP polymers exhibited significant increase/decrease in surface capping when compared with the control groups. The PVP- and PEG-based surface capping provide steric repulsion to the nanoparticles. It has been well reported in the previous studies that the basic aim of organic coating in the form of polymers and stabilizers was to stabilize AgNPs against aggregation. This aggregate formation is hindered by the presence of an organic layer under various conditions or in a certain stage of nanoparticle growth. The overall fate of the coated AgNPs is generally controlled by the properties of the shell that is formed around the Ag core (Dallas et al. 2011; Eising et al. 2011). We report similar effects of polymer-induced steric repulsion for PEG- and PVP-treated AgNPs which modulated its stability in colloids.

Citrate-AgNPs are known to have greater aggregation kinetics and less stability, which limits its biological applications (Gutierrez et al. 2015); in the current study, plant extract-derived functional groups conferred stability to citrate-AgNPs and its derivatives. However, the group remained less heat resistant when compared with HC-AgNPs derivatives.

The time-dependent stability results in colloid suggest the increase in absorbance intensity at 4th month and 8th month. This suggests the shift toward mono-dispersed NPs from polydispersed ones. The absorbance increase is in accordance with the previous studies where the absorbance value of λ_{\max} for colloidal AgNPs stabilized after 29 days (Pinto et al. 2010). Other studies have also shown that the presence of ions effectively destabilizes the citrate-AgNPs, leading to time-dependent aggregation (Huynh and Chen 2011). Our aging-dependent results suggested an increase in FWHM of citrate-AgNPs and HC-AgNPs at 8th month.

PEG-20, PVP-40, 2CPVP-20, and HC-AgNPs showed blueshift in the absorption spectrum, suggesting a decrease in particle size as a function of removal of the outer capping layer when heated. CPEG-40 AgNPs, and PVP-40 AgNPs showed the highest heat resistance as no significant FWHM and λ_{\max} change was observed following the heat treatment. High temperatures up to 100°C were used by many researchers during AgNPs assembly using bio-polymers and plant extracts (El-Rafie et al. 2011; Fayaz et al. 2009). However, CPEG-40 AgNPs and PVP-40 AgNPs showed highest heat resistance as no significant FWHM and λ_{\max} change was observed following heating at high temperature. This could be due to the presence of high amount of surface coating for CPEG-40 AgNPs and PVP-40 making NPs more susceptible to heat degradation.

Previous studies report the effect of aging on AgNPs through flower-like structure development from spherical (Zonooz and Salouti 2011). Similarly, the redshift in λ_{\max} for 2CPVP-80 at 8th month could be due to the surface shape changes. Yin et al. assessed λ_{\max} shifts in AgNPs through experiments and by simulation. Their results suggested that as the degree of oxidation of NPs increased the absorbance intensity decreased and a redshift in the λ_{\max} was observed (Yin et al. 2002).

Out of these, only PVP-40 AgNPs, CPVP-80 AgNPs, and 2CPEG-5 AgNPs showed a considerable decrease in FWHM, implying colloidal stability with time. We thereby report these three screened AgNPs for long-term stability studies, based on aging and heat resistance.

It is now well accepted that silver nanoparticles acquired protein corona after contact with the biological media (Tenzer et al. 2013), and hence, in order to use these NPs in close proximity with a biological system, details regarding surface capping, structure, and colloidal behavior are very important. The comparative study in three different cell lines showed that 0.5 HC AgNPs exhibited different cellular uptake and proliferation in each cell line. The uptake of 0.5 HC-AgNPs was high in MCF-7 cell lines as all the concentrations used exhibited significant decrease in viability, even at 0.5 mg/mL concentration. This decrease in viability was noted at 1.5 mg/mL concentration in the rest of the two studied cell lines.

Conclusion

In the current study, we adopted a surface chemistry-based steric repulsion approach to investigate the colloidal stability of HC-AgNPs and determine its application as a commercial antibacterial formulation. The AgNPs in our studies did not exhibit cytotoxicity less than 50%, and hence, there is little evidence of biotransformation of AgNPs. The AgNPs presenting the viability of more than 90% can be

safely used as drug carrier agents. However, more studies regarding cytotoxicity, viability, and safety together with dose-dependent response are essential to justify their use prior to commercial and anti-microbial applications. The high stability (up to eight months) and heat resistance of AgNPs provide promising evidence for the commercial application of HC-AgNPs as antimicrobial agent. The *in vitro* safety and limited evidence of biotransformation suggest that HC-AgNPs could be used effectively for biomedical applications. The current study provides a road map for modulating the surface capping of biological nanoparticles and assesses its corresponding effect on the stability.

Acknowledgements The authors would like to acknowledge Atta ur Rehman School of Biosciences, NUST for funding the current research, Department of Chemistry, SBASSE, LUMS for characterization of nanoparticles.

Funding The authors are grateful to ASAB-NUST for MS student's research funds to run this project.

Data availability The data that support our studies are available from the corresponding authors on request.

Compliance with ethical standards

Conflict of interest All the authors declared no conflict of interest in the current research.

References

- Afshinnia K, Sikder M, Cai Bo, Baalousha M (2017) Effect of nanomaterial and media physicochemical properties on Ag NM aggregation kinetics. *J Colloid Interface Sci* 487:192–200
- Ashraf S, Abbasi AZ, Pfeiffer C, Hussain SZ, Khalid ZM, Gil PR, Parak WJ, Hussain I (2013) Protein-mediated synthesis, pH-induced reversible agglomeration, toxicity and cellular interaction of silver nanoparticles. *Colloids Surf B* 102:511–518
- Banerjee S, Loza K, Meyer-Zaika W, Prymak O, Epple M (2014) Structural evolution of silver nanoparticles during wet-chemical synthesis. *Chem Mater* 26:951–957
- Brown AN, Smith K, Samuels TA, Jiangrui Lu, Obare SO, Scott ME (2012) Nanoparticles functionalized with ampicillin destroy multiple-antibiotic-resistant isolates of *Pseudomonas aeruginosa* and *Enterobacter aerogenes* and methicillin-resistant *Staphylococcus aureus*. *Appl Environ Microbiol* 78:2768–2774
- Brown PK, Qureshi AT, Moll AN, Hayes DJ, Todd W et al (2013) Silver nanoscale antisense drug delivery system for photoactivated gene silencing. *ACS Nano* 7:2948–2959
- Dallas P, Sharma VK, Zboril R (2011) Silver polymeric nanocomposites as advanced antimicrobial agents: classification, synthetic paths, applications, and perspectives. *Adv Coll Interface Sci* 166:119–135
- de Barros C, Nasi H, Cruz GCF, Mayrink W, Tasic L (2018) Bio-based synthesis of silver nanoparticles from orange waste: effects of distinct biomolecule coatings on size, morphology, and antimicrobial activity. *Nanotechnol Sci Appl* 11:1
- Eising R, Signori AM, Fort S, Domingos JB (2011) Development of catalytically active silver colloid nanoparticles stabilized by dextran. *Langmuir* 27:11860–11866
- El-Rafie MH, El-Naggar ME, Ramadan MA, Fouda MMG, Al-Deyab SS, Hebeish A (2011) Environmental synthesis of silver nanoparticles using hydroxypropyl starch and their characterization. *Carbohydr Polym* 86:630–635
- El-Shishtawy RM, Asiri AM, Al-Otaibi MM (2011) Synthesis and spectroscopic studies of stable aqueous dispersion of silver nanoparticles. *Spectrochim Acta Part A Mol Biomol Spectrosc* 79:1505–1510
- Badawy El, Amro M, Silva RG, Morris B, Scheckel KG, Suidan MT, Tolaymat TM (2010) Surface charge-dependent toxicity of silver nanoparticles. *Environ Sci Technol* 45:283–287
- Fayaz AM, Balaji K, Kalaichelvan PT, Venkatesan R (2009) Fungal based synthesis of silver nanoparticles—an effect of temperature on the size of particles. *Colloids Surf B* 74:123–126
- Gericke M, Pinches A (2006) Biological synthesis of metal nanoparticles. *Hydrometallurgy* 83:132–140
- Gutierrez L, Aubry C, Cornejo M, Croue J-P (2015) Citrate-coated silver nanoparticles interactions with effluent organic matter: influence of capping agent and solution conditions. *Langmuir* 31:8865–8872
- Haberl N, Hirn S, Wenk A, Diendorf J, Epple M, Johnston BD, Krombach F, Kreyling WG, Schleh C (2013) Cytotoxic and proinflammatory effects of PVP-coated silver nanoparticles after intratracheal instillation in rats. *Beilstein J Nanotechnol* 4:933–940
- Hoppe CE, Lazzari M, Pardiñas-Blanco I, Arturo López-Quintela M (2006) One-step synthesis of gold and silver hydrosols using poly(*N*-vinyl-2-pyrrolidone) as a reducing agent. *Langmuir* 22:7027–7034
- Hotze EM, Phenrat T, Lowry GV (2010) Nanoparticle aggregation: challenges to understanding transport and reactivity in the environment. *J Environ Qual* 39:1909–1924
- Huynh KA, Chen KL (2011) Aggregation kinetics of citrate and polyvinylpyrrolidone coated silver nanoparticles in monovalent and divalent electrolyte solutions. *Environ Sci Technol* 45:5564–5571
- Kelly KL, Coronado E, Zhao LL, Schatz GC (2003) The optical properties of metal nanoparticles: the influence of size, shape, and dielectric environment. ACS Publications, New York
- Khan F, Hashmi MU, Khalid N, Hayat MQ, Ikram A, Janjua HA (2016) Controlled assembly of silver nano-fluid in *Heliotropium crispum* extract: A potent anti-biofilm and bactericidal formulation. *Appl Surf Sci* 387:317–331
- Kvitek L, Panáček A, Soukupova J, Kolář M, Večeřová R, Prucek R, Holecova M, Zbořil R (2008) Effect of surfactants and polymers on stability and antibacterial activity of silver nanoparticles (NPs). *J Phys Chem C* 112:5825–5834
- Levard C, Matt Hotze E, Lowry GV, Brown GE, Jr. (2012) Environmental transformations of silver nanoparticles: impact on stability and toxicity. *Environ Sci Technol* 46:6900–6914
- Morgan E, Wupperfeld D, Morales D, Reich N (2019) Shape matters: Gold nanoparticle shape impacts the biological activity of siRNA delivery. *Bioconjug Chem* 30:853–860
- Mulfinger L, Solomon SD, Bahadory M, Jeyarajasingam AV, Rutkowski SA, Boritz C (2007) Synthesis and study of silver nanoparticles. *J Chem Educ* 84:322
- Piao MJ, Kang KA, Lee IK, Kim HS, Kim S, Choi JY, Choi J, Hyun JW (2011) Silver nanoparticles induce oxidative cell damage in human liver cells through inhibition of reduced glutathione and induction of mitochondria-involved apoptosis. *Toxicol Lett* 201:92–100
- Pinto VV, Ferreira MJ, Silva R, Santos HA, Silva F, Pereira CM (2010) Long time effect on the stability of silver nanoparticles in aqueous medium: effect of the synthesis and storage conditions. *Colloids Surf A* 364:19–25

- Qiu L, McCaffrey R, Zhang W (2018) Synthesis of metallic nanoparticles using closed-shell structures as templates. *Chem Asian J* 13:362–372
- Rajput S, Werezuk R, Lange RM, McDermott MT (2016) Fungal isolate optimized for biogenesis of silver nanoparticles with enhanced colloidal stability. *Langmuir* 32:8688–8697
- Ravindran A, Chandran P, Sudheer Khan S (2013) Biofunctionalized silver nanoparticles: advances and prospects. *Colloids Surf B* 105:342–352
- Romer I, White TA, Baalousha M, Chipman K, Viant MR, Lead JR (2011) Aggregation and dispersion of silver nanoparticles in exposure media for aquatic toxicity tests. *J Chromatogr A* 1218:4226–4233
- Römer I, White TA, Baalousha M, Chipman K, Viant MR, Lead JR (2011) Aggregation and dispersion of silver nanoparticles in exposure media for aquatic toxicity tests. *J Chromatogr A* 1218:4226–4233
- Sastry M, Mayya KS, Bandyopadhyay K (1997) pH Dependent changes in the optical properties of carboxylic acid derivatized silver colloidal particles. *Colloids Surf A* 127:221–228
- Sharma VK, Siskova KM, Zboril R, Gardea-Torresdey JL (2014) Organic-coated silver nanoparticles in biological and environmental conditions: fate, stability and toxicity. *Adv Colloid Interface Sci* 204:15–34
- Srikar SK, Giri DD, Pal DB, Mishra PK, Upadhyay SN (2016) Green synthesis of silver nanoparticles: a review. *Green Sustain Chem* 6:34
- Suman TY, Radhika Rajasree SR, Kanchana A, Beena S, Elizabeth. (2013) Biosynthesis, characterization and cytotoxic effect of plant mediated silver nanoparticles using *Morinda citrifolia* root extract. *Colloids Surf B* 106:74–78
- Tenzer S, Docter D, Kuharev J, Musyanovych A, Fetz V, Hecht R, Schlenk F, Fischer D, Kiouptsi K, Reinhardt C (2013) Rapid formation of plasma protein corona critically affects nanoparticle pathophysiology. *Nat Nanotechnol* 8:772
- Yin Y, Li Z-Y, Zhong Z, Gates B, Xia Y, Venkateswaran S (2002) Synthesis and characterization of stable aqueous dispersions of silver nanoparticles through the Tollens process. *J Mater Chem* 12:522–527
- Zhang H, Smith JA, Oyanedel-Craver V (2012) The effect of natural water conditions on the anti-bacterial performance and stability of silver nanoparticles capped with different polymers. *Water Res* 46:691–699
- Zonooz NF, Salouti M (2011) Extracellular biosynthesis of silver nanoparticles using cell filtrate of *Streptomyces* sp. ERI-3. *Sci Iran* 18:1631–1635

Publisher's Note Springer Nature remains neutral with regard to jurisdictional claims in published maps and institutional affiliations.